Photoluminescence and Raman Spectroscopy of Single Diamond Nanoparticle

J.Y. WANG, T.Y. KO and K.W. SUN*
Department of Applied Chemistry and Institute of Molecular Science, National Chiao Tung University, Hsinchu 30010, China

Abstract — **The paper reports the techniques that we have devised for immobilizing and allocating a single nanodiamond on the electron beam (E-beam) patterned smart substrate. The properly designed coordination markers on the semiconductor substrate and the high throughput of the confocal microscope provide us with a convenient tool to single out a nanodiamond with a size less than 100 nm and to study its optical properties on a single nanostructure basis. We have observed a broad PL emission centered at about 700 nm from a single nanodiamond which is due to the defects, vacancies in the nanodiamonds or the disordered carbon layer covered on the nanodiamond surface. We also observe red-shift in energy and asymmetrical broadening in linewidth of the sp^3 bonding Raman peak when the size of the single nanodiamond is decreased.**

I. INTRODUCTION

Nanometer-sized diamond possesses not only the properties of high thermal conductivity, hardness, electrical resistivity and strength as the bulk diamond but also other properties such as special optical properties and magnetoresistivity [1]. It has recently attracted intense interest in expectation of the possession of outstanding properties different from those of bulk diamond. In particular, nanodiamonds are expected to be used for a variety of applications, such as in solving applied problems in biology, protein chemistry, molecular biology, etc.. Conventional organic fluorophores suffered from poor photo stability, narrow absorption spectra and broad emission features. Recent advances in the synthesis of the semiconductor nanocrystals have resulted in biomarkers which are brighter, more sensitive, photo-stable and biocompatible [2-4].

It is recently demonstrated that diamonds with a nominal size of 100 nm are capable of producing stable fluorescence from color centers after surface treatment with strong oxidative acids [5]. More recently, sub-100 nm nanodiamonds with nitrogen point defects have been used as single-particle biomarkers in experiments of fixed and live Hela cells [6]. The fluorescent nanodiamonds could possibly be used as a fluorescent biomarker for in vitro as well as in vivo studies at the single-particle level. In addition, many studies have been motivated by the tremendous technological potential for diamond system composed of nanometer-sized crystalline [6-9]. Although there have been a number of reports on the optical properties of nanodiamonds, however, most of their studies focus on diamond nanoparticles in cluster or powder form [10-12].

In this work, we report the photoluminescence and Raman spectroscopy studies of a single free standing nanodiamond immobilized on a Si substrate under laser excitation at 532 nm using techniques of combining a confocal microscope and an electron-beam (e-beam) lithography techniques. The Raman line of the single naodiamond is shifted and broadened relative to that of nature diamond which occurs at 1332.5 cm^{-1} and has a linewidth of 2 cm^{-1} [13]. We have examined the finite-size effects on the frequency shift and linewidth of the phonon peaks in Raman spectra based on phonon-confinement models [14].

II. PREPARATION OF SINGLE NANODIAMOND AND NANOSTRUCTURED SMART SUBSTRATE

The nanodiamond powder used in this study is commercially available (GE Diamond Company) and is all synthesized under high pressure and high temperature (HPHT) with an average size of about 100 nm and 40 nm and with a size distribution within ~ 20%, respectively. The x-ray diffraction and transmission electron microscopy (TEM) analysis reveal that the diamond sample under investigation has crystalline structure. We first dilute the nanodiamond powder in DI water and ethanol mixture. The solution is then placed in an ultrasonic bath operated at a vibration frequency of 185 KHz for 30 minutes to prevent the formation of the nanodiamond clusters. Due to the acoustic cavitation effect [15], the ultrasonic wave heats up the water and breaks the water molecules into H^+ and OH^- ions. The OH^- ions attach onto the nanodimond surface and induce a Coulomb repulsion force between nanoparticles. Therefore, the clustering of nanodiamonds can be avoided.

A test drop of the solution is placed on a bare Si wafer and, after the solution dries out, the scanning electron microscope (SEM) images are taken to examine the clustering of the nanodiamond. The concentration of the solution is continuously adjusted until the nanoparticles can be well dispersed and separated on the template (as shown in Figure 1). The preparation of the patterned smart substrates is explained as follows.

978-1-4244-1573-1/08/$25.00 ©

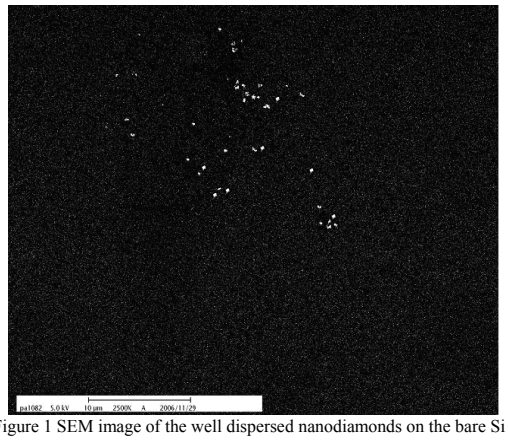

Figure 1 SEM image of the well dispersed nanodiamonds on the bare Si surface.

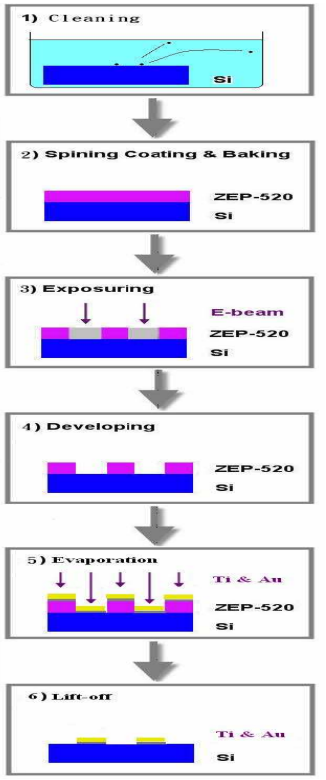

Figure 2 Lithography steps for making the coordination markers on Si.

A Si wafer is diced into 2 cm by 2 cm chips. A pattern of two dimensional arrays of round metal dots with diameter of 300 nm and pitch size of 1.2 μm is defined on the Si chip using electron beam (E-beam) lithography technique within an area of 180 μm by 30 μm. For each fifth dot, we make a square shape instead of a round one so that the coordinates can be easily counted under an optical microscope. Figure 2 shows the E-beam lithography steps for making the Si template with coordination markers.

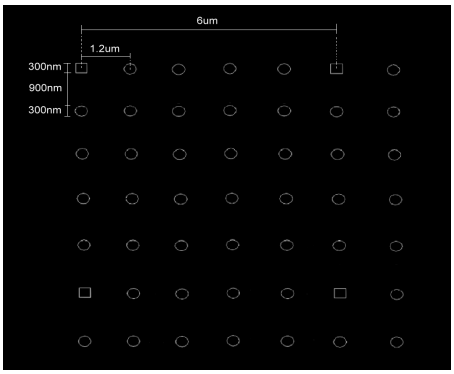

Figure 3 SEM image of the E-beam defined pattern of coordination markers.

The array of coordination marker pattern is then repeated several times to cover an area of abut 0.3 by 0.6 mm^2 on the chip. The pitch and metal dot sizes are determined according to the laser spot size (~ 1 μm) and the optical resolution of our confocal microscope (~ 300 nm) at the excitation wavelength of 532 nm. Figure 3 and 4 show the scanning electron microscope (SEM) images of the patterned substrates.

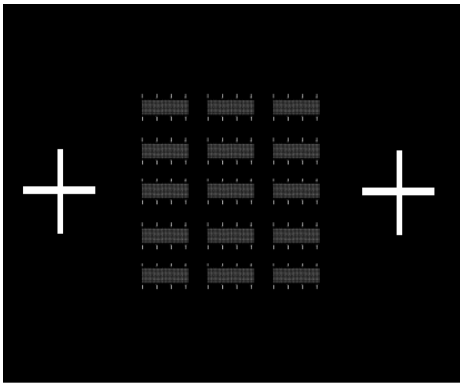

Figure 4 SEM image of the2D coordination marker arrays...

A drop of the well diluted nanodiamond solution is placed on the patterned template. After the sample dries out, the surface is scanned with SEM to allocate a single nanodimaond. Figure 5 shows the SEM scanning results of two separated single nanodiamonds with a size of 90 nm and 35 nm (indicated by the yellow arrow lines in the figure), respectively. Most importantly, from the SEM image, we can ensure that there is no other nanodiamond within the laser focus spot but the selected target before the optical measurements.

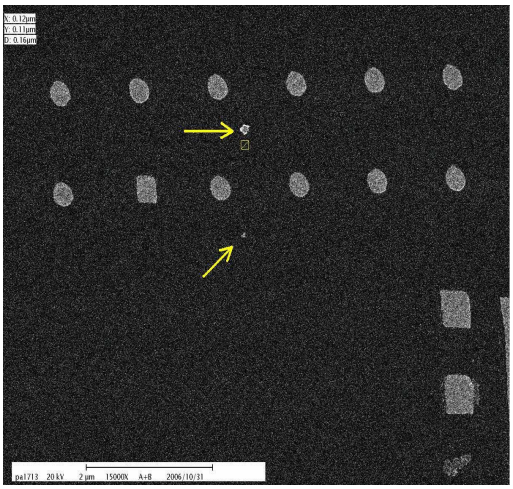

Figure 5 SEM images of the single 90 nm (the upper one) and 35 nm (the lower one) nanodiamonds near the coordination markers.

III. PHOTOLUMINESCENCE AND RAMAN SPECTROSCOPY MEASUREMENTS

After a single nanodiamond is allocated from the SEM images and a corresponding coordinate is assigned. The dimension of the coordination markers is properly designed so that they can still be clearly seen under the optical microscope. The entire template is moved via an X-Y stepping motor to the given coordinate to position the targets under the laser spot while the optical image of the substrate is simultaneously monitored on a TV screen. The laser beam focused through the microscope objective with a spot size of 1 μm is moved to the given coordinate where the single nanodiamond is located. The PL and Raman signals are collected through the same objective and are analyzed by a 0.32 m spectrometer equipped with a liquid nitrogen cooled CCD detector at excitation wavelength of 532 nm. The optical signal can be further optimized by adjusting the focal plane position along the z-axis via the piezo-driven objective lens. The acquired spectra are averaged several times until a good signal-to-noise ratio is achieved. We measured photoluminescence from a single diamond nanoparticle. We also collected Raman signal from a single nanodiamond with sizes of 90 and 35 nm, respectively.

IV. RESULTS AND DISCUSSION

A broad PL emission centered at about 700 nm was observed from the single nanodiamond at excitation wavelength of 532 nm as shown in Figure 6. The features on this broad emission can be fitted with three Lorentzian peaks centered at 637 nm, 671 nm and 714 nm, respectively. Similar PL results were reported by Glinka et al. [16] on diamond powder excited with UV laser light. The different emission peaks originate from diamond surface defect, vacancies and impurities attached on the surface. Those impurities include nitrogen, boron and carbon with graphite structures.

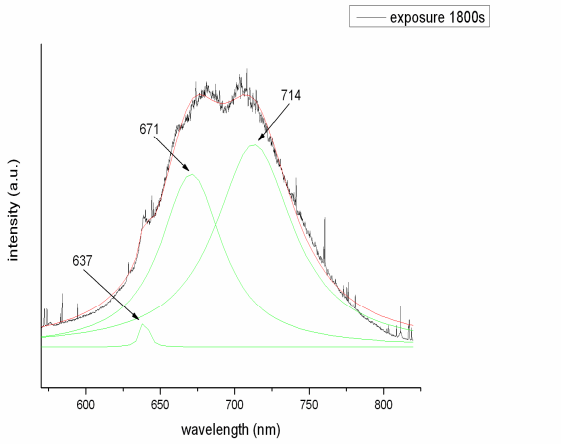

Figure 6 Photoluminescence spectra from the 90 nm single nanodiamond.

For the single 90 nm nanodiamond, a Raman peak due to the sp^3 bonding structure in the diamond was detected at the energy of 1329 ± 1.5 cm^{-1} (with a 2400 groove grating) with a linewidth of ~ 10 cm^{-1} as shown in Figure 7. This peak is red-shifted by ~ 3 cm^{-1} in compared to the bulk diamond.

The Raman spectrum from the single 35 nm nanodiamond, as shown in Figure 6, shows a Raman peak at ~ 1325 ± 1.5 cm^{-1}. Be noted that its lineshape looks asymmetric and is broaden to 80 cm^{-1}. A strong Raman signature from the D, G bands also appears at the energy of ~ 1600 cm^{-1}. Its intensity is comparable to the sp^3 Raman peak, which indicates that this single 35 nm diamond may contain higher percentage of graphite structure than the 90 nm one. Therefore, the true size of the 35 nm single

nanodimond with sp^3 structures should be smaller than the size determined from the SEM image.

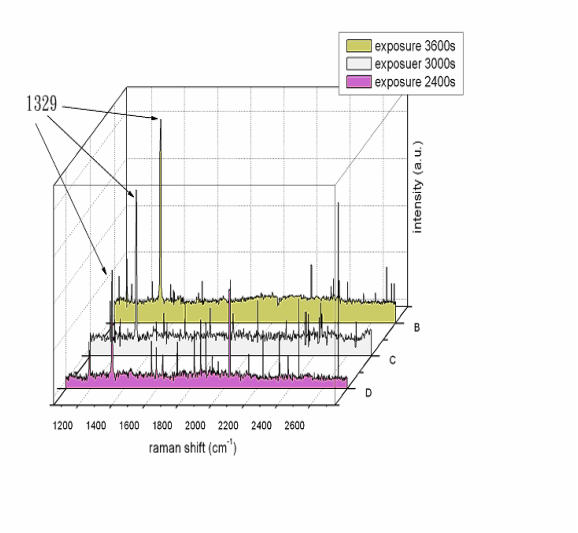

Figure 7 Raman spectra from single 90 nm diamond with integration time of 2400 sec, 3000 sec and 3600 sec, respectively

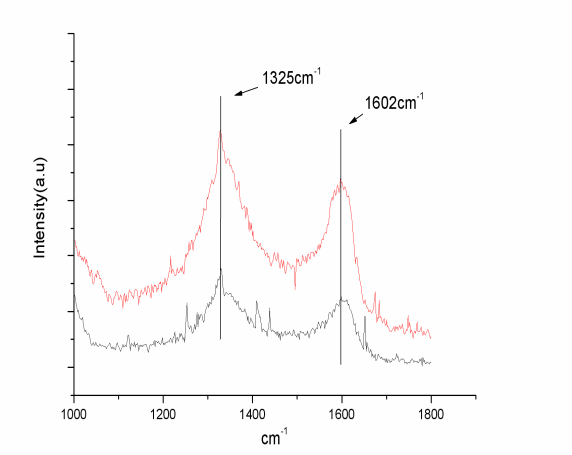

Figure 8 Raman spectra from single 35 nm diamond with integration time of 2400 sec and 3600 sec, respectively

A theoretical model (known as the phonon-confinement model) was first proposed by Richter et al. [14] to explain the observed shift to lower frequency and broadening of Raman line in microcrystalline Si. More recently, results of phonon-confinement calculations in diamond were reported in Ref. [17-19]. The phonon-confinement model is based on the fact that, in an infinite crystal, crystal momentum conversation limits Raman spectroscopy to observe phonons at the Brillouin zone center (q = 0). However, phonon can be confined in space by microcrystal boundaries in a crystal with finite size. This leads to uncertainty in the phonon momentum which allows phonons with q > 0 to contribute to the Raman signal. When the momentum uncertainty is convolved with the dispersion curve, the calculated Raman line shape becomes asymmetrically broadened and the maximum shifts to lower frequency as the particle size decreases. The calculated results reported by Yoshikawa et al. [18] predicates that the sp^3 Raman peak of ~ 5 nm diamond particles shows red-shift of ~ 13 cm^{-1} in energy and linewidth larger than 50 cm^{-1}. For the same particle size, a shift as large as ~ 6 cm^{-1} and asymmetric line shape and larger broadening of the calculated Raman line were also reported by Ager et al. [19].

In our studies, the linewidth broadening arises from averaging over particles with different size can be ruled out because only the single particle is investigated. The observed energy red-shift and linewidth broadening of the Raman peak in our experiments are attributed to the phonon-confinement effects and are in qualitatively agree with the above theoretical models. The difference in the amount of energy shift and linewidth broadening in compared to the calculations can be explained by the irregular shape of the nanodiamond, which should lead to the complications in the calculations, as well as the determination of the true particles size with sp^3 structures.

V. CONCLUSION

In summary, by combining a confocal microscope and an e-beam patterned smart substrate, we are able to study optical properties of a single nanodiamond with a size of less than 100 nm. A broad emission centered at about 700 nm is observed in the PL spectra due to the defects, vacancies in the nanodiamonds or the disordered carbon layer covered on the nanodiamond surface. The observed energy red-shift and asymmetrical linewidth broadening of the Raman peak in the experiments as the nanoparticle size decreases are attributed to the phonon-confinement effect. In contrast to earlier reports on nanodiamond powder or clusters, the factors arising from size distribution can be ruled out and the results can be compared with calculations in parallel.

ACKNOWLEDGEMENT

This work was supported by the National Science Council of Republic of China under contract No. NSC 96-2112-M-009- 024 –MY3 and the MOE ATU program.

REEFERENCES

[1] N.R. Greiner, D.S. Phillips, Johnson and F. Volk, 1998 Nature (London) **333,** 440 (1998).
[2] X. Michalet, F. Pinaud, T, D. Lacoste, M. Dahan, M. Bruchez, A. P. Alivisatos, S. Weiss, Single Mol. **2**, 261-276 (2001).
[3] B. O. Dabbousi, J. Rodriguez-Viejo, F. V. Mikulec, J. R. Heine, H. Mattoussi, R. Ober, K. F. Jensen, M. J. Bawendi, Phys. Chem. B **101**, 9463-9475 (1997).
[4] M. A. Hines, P. J. Guyot-Sionnest, Phys. Chem. **100**, 468-471 (1996).
[5] S.J. Yu, M.W. Kang, H.C. Chang, K.M. Chen, Y.C. Yu , J. Am. Chem. Soc. **127,** 17604 (2005).
[6] C.C. Fu, H.Y. Lee, K. Chen, T.S. Lim, H.Y. Wu, P.K. Lin, P.K. Wei, P.H. Tsao, H.C. Chang, W. Fann, PNAS **104,** 727 (2007).
[7] W.A.Yarbrough and A.B. Sawaoka, Carbon **32**, 665 (1990).
[8] F. Davanloo, T.J. Lee, J.H. You and C.B. Collins, J. Mater. Res. **8** 3090 (1993).
[9] V.F. Dorfman, Thin Solid Films **212,** 267 (1992).
[10] J. Filik, J.N. Harvey, N.L. Allan, P.W. May, Phys. Rev. B **74,** 035423 (2006).
[11] F.L. Zhao, Z. Gong, S.D. Liang, N.S. Xu, S.Z. Deng, J. Chen, H.Z. Wang, Appl. Phys. Lett. **85,** 914 (2004).
[12] J. Chen, S.Z. Deng, J. Chen, Z.X. Yu, N.S. Xu, Appl. Phys. Lett. **74,** 3651 (1999).
[13] S.A. Solin and A.K. Ramdas, Phys. Rev. B **1**,1687 (1970).
[14] H. Richer, Z. P. Wang, and L. Ley, Solid State Commun. **39**, 625 (1981
[15] T. Uchida, T. Sato, S. Takeuchi, N. Kuramochi and N. Kawashima, Jpn. J. Appl. Phys. **42**, 2967-2970 (2003).
[16] Yu. D. Glinka, K.-W. Lin, H.-C. Chang, and S. H. Lin, J. Phys. Chem. B**,** 103, 4251 (1999**)**
[17] M. Yoshikawa, Y. Mori, H. Obata, M. Maegawa, G. Katagiri, H. Ishida, A. Ishitani, Appl. Phys. Lett. **67**, 694-696 (1995).
[18] J. W. Ager III, D. Kirk Veirs, and G. M. Rosenblatt, Phys. Rev. B **43**, 6491 (1991).
[19] M. Yoshikawa, Y. Mori, M. Maegawa, G. Katagiri, H. Ishida, and A. Ishitani, Appl. Phys. Lett., **1993**, 62, 3114-3116.

*Corresponding Author; email:kwsun@mail.nctu.edu.tw; Tel: 886-3-571121ext56581, FAX: 886-3-5131248